Self-assembling lipid modified glycol-split heparin nanoparticles suppress lipopolysaccharide-induced inflammation through TLR4-NF-κB signaling.

AUTHOR(S):

Babazada, Hasan; Yamashita, Fumiyoshi; Yanamoto, Shinya; Hashida, Mitsuru

CITATION:

Babazada, Hasan ...[et al]. Self-assembling lipid modified glycol-split heparin nanoparticles suppress lipopolysaccharide-induced inflammation through TLR4-NF-κB signaling.. Journal of controlled release 2014, 194: 332-340

ISSUE DATE:

2014-11-28

URL:

http://hdl.handle.net/2433/191264

Self-assembling lipid modified glycol-split heparin nanoparticles suppress lipopolysaccharide-induced inflammation through TLR4–NF-κB signaling

Hasan Babazada[1], Fumiyoshi Yamashita[1], Shinya Yanamoto[1] and Mitsuru Hashida[1, 2*]

[1]Department of Drug Delivery Research, Graduate School of Pharmaceutical Sciences, Kyoto University, Yoshidashimoadachi-cho, Sakyo-ku, Kyoto 606-8501, Japan.

[2]Institute for Integrated Cell-Material Sciences, Kyoto University, Yoshidaushinomiya-cho, Sakyo-ku, Kyoto 606-8501, Japan.

*Corresponding author info:
Tel: 81-75-753-4535
Fax: 81-75-753-4575
E-mail: hashidam@pharm.kyoto-u.ac.jp

Conflict of interest

Authors declare no conflict of interest.

Keywords:
Inflammation
Heparin nanoparticles
Toll-like receptors
Desulfation
Macrophage
Nuclear factor-κB

Abstract

Self-assembling heparin nanoparticles have attracted much attention as promising drug carriers for various drugs, genes and imaging agents. In the present investigation, we found that heparin nanoparticles are selective Toll-like receptor 4 (TLR-4) antagonists and have a much greater anti-inflammatory effect than native heparin. More specifically, we developed self-assembling nanoparticles composed of glycol-split heparin/D-erythro-sphingosine conjugates (NAHNP), characterized their physicochemical properties and anti-inflammatory effect *in vitro*. Unlike native heparin, NAHNP significantly inhibited lipopolysaccharide-induced activation of MyD88 - dependent NF-κB signaling pathway and production of pro-inflammatory cytokines such as TNF-alpha from mouse macrophages with IC50= 0.019 mg/mL. Furthermore, we investigated the structure–activity relationship of the conjugates and identified the length of attached alkyl chains of D-erythro-sphingosine to be critical for anti-inflammatory effect. Decrease in alkyl chain length of NAHNP resulted in loss of inhibitory activity. In line with these findings, 6-O-sulfate groups of D-glucosamine residue were essential for effective inhibition, while removal of 2-O-sulfo and 3-O-sulfo groups as well as replacement of N-sulfo groups with N-acetyl did not alter anti-inflammatory activity. Therefore, NAHNP would be a promising candidate in acute and chronic inflammatory disorders, in addition to the nature of a drug carrier.

1. Introduction

Polymeric or macromolecular micelles have extensively been studied as vehicles for targeted delivery of various drugs, genes and imaging agents. The micelles are self-assembled colloidal particles comprising amphiphilic molecules such as two-block copolymers and lipid-grafted macromolecules. Among many carrier systems that have been developed, heparin-based nanoparticles are one of the attractive ones [1]. As in the case of other materials, coating of nanoparticles with heparin can suppress complement- mediated opsonization [2, 3], and prolong retention in blood circulation [4]. Heparin-based nanoparticles have been applied as carriers for anti-cancer drugs [5], oxygen [6, 7] and anti-inflammatory metallic particles such as gold and silver [8]. Combination of heparin with pH-sensitive [9, 10] or temperature sensitive [11] polymers or with magnetically operatable nanoparticles [12] has also been investigated for targeted drug delivery. In addition to low toxicity and high biocompatibility, heparin has a variety of biological activities beyond anti-coagulation [13–15]. The intrinsic properties of heparin can provide additional functionality towards particulate carrier systems. One typical example is anti-angiogenic therapy to suppress tumor growth [16, 17]. Lipid-conjugated heparin derivatives retain an ability to bind to angiogenic factors such as fibroblast growth factors and vascular endothelial growth factors, so that they can significantly decrease endothelial cell proliferation [18, 19]. Another interesting property of heparin is its anti-inflammatory activity [13], although there is a lack of related reports dealing with heparin-based nanoparticles [8]. Heparin can bind and inhibit proteins critically involved in inflammation, such as cytokines, growth factors, cytotoxic peptides, and tissue-destructive enzymes, thereby limiting the activation of inflammatory cells [13, 14]. It has been reported to be useful in inflammatory conditions such as arthritis [20], inflammatory bowel disease [21] and allergic rhinitis [22]. However, the clinical application of heparin for these conditions is limited by its anticoagulant effect or non-specificity of action [15]. Underlying mechanisms responsible for the anti-inflammatory effect of heparin are yet to be clarified [23], but notably heparin inhibits recruitment of leukocytes to inflammatory sites via blockade of P- and L-selectins which critically requires 6-O sulfation of glucosamine residues [24]. Furthermore, heparin inhibits adhesion and migration of leukocytes in the endothelium by binding to cell surface proteins such as β2-integrin adhesion molecule CD11b/CD18 and platelet/endothelial cell-adhesion molecule 1 [15]. In this study, we demonstrate that self-assembling nanoparticles composed of glycol-split non-anticoagulant heparin–D-erythro-sphingosine conjugates (NAHNP) are selective Toll-like receptor 4 (TLR4) antagonists and have a much greater anti-inflammatory activity than native heparin. This means that the heparin nanoparticles can block an initial step of pro-inflammatory reactions in primitive immune cells which is a different target from that of the above-mentioned action. TLR family members are critical for the development of innate and adaptive immunity in response to pathogens and endogenous ligands generated in damaged tissues [25]. TLRs, particularly

signaling through TLR4 have also been implicated in both the establishment of diseases such as arthritis [26], Alzheimer's disease [27], chronic myositis [28], and systemic lupus erythematosus [29] and their maintenance. Under circumstances when the immune system is disbalanced, inhibition of TLR4 signaling appears to be important in limiting the redundant response during the inflammation. Here we found that NAHNP blocks the production of tumor necrosis factor (TNF-α) from *Escherichia coli* lipopolysaccharide (LPS)-mediated stimulation of macrophages in vitro. Macrophages as essential cells of the innate immune system are a major source of pro-inflammatory cytokines after stimulation with LPS, a selective TLR4 agonist [30, 31]. In vitro experiments of the underlying mechanism using mouse macrophages suggested that the inhibitory effect of nanoparticles was due to the downregulation of MyD88-dependent nuclear factor-κB (NF-κB) signaling via TLR4 but not other TLRs. In addition, we investigated the structure–activity relationship for the anti-inflammatory effects and elucidated functional groups in NAHNP needed for the activity. These results shed light on synergistic effects of anti-inflammatory drugs with the heparin-based nanoparticulated carriers.

2. Materials and methods

2.1. Synthesis of glycol-split non-anticoagulant heparin D-erythro-sphingosine nanoparticles (NAHNP)

Glycol-split non-anticoagulant heparin (NAH) was obtained by periodate-oxidation and borohydride-reduction of heparin (Nacalai Tesque, Inc., Kyoto, Japan) as described in the well-established method of Conrad et al. [32]. NAH then was dissolved in formamide with different amounts of 1-ethyl-3-(3-dimethylaminopropyl)-carbodiimide followed by the addition of different molarities of D-erythro-sphingosine (LKT Laboratories, Inc., St. Paul, MN) dissolved in dimethylformamide. 1-ethyl-3-(3-dimethylaminopropyl) carbodiimide was maintained at a ratio of 5:1 with D-erythro-sphingosine. The reaction mixture was stirred at room temperature for 24 h under a nitrogen atmosphere. Afterwards, the reaction mixture was precipitated in pure ethanol, centrifuged 14,000 ×g for 10 min followed by decantation. This was repeated 3 times to remove any remaining unreacted D-erythro-sphingosine and reaction solutions. Precipitates were then dried in a vacuum and lyophilized as NAHNP. Self-assembled nanoparticles of NAHNP were prepared by ultrasonication using a probe sonicator (UD-201, Tomy Seiko Co. Ltd., Japan) for 1 min in distilled water. Unfractionated heparin was used instead of NAH to synthesize native heparin nanoparticles (HPNP). 1H-NMR spectra were obtained with JEOL 400 spectrometers at 400 MHz (D_2O : ethanol-D6 = 2.5:1 v/v). In NAH, the C2-C3 bond of glucuronic acid is cleaved resulting in a shift in the H-2 and H-3 peaks (s, δ=3.38 ppm) of glucuronic acid causing them to shift under the peak of 6-O-sulfoglucosamine H-2 (s, δ = 3.27 ppm). Chemical shifts for attached D-erythro-sphingosine were assigned: δ = 1.09 (t, H18, -CH3), 1.13 (m, H-7-H-17, -CH2 −), 2.90 (s, H-2), 3.61 (s,

H-1), 5.53 (s, H-4), 5.78 (s, H-5), 8.04 (s, CO-NH). Degree of substitution with D-erythro-sphingosine was estimated using a direct titration method as described elsewhere [33].

2.2. Synthesis of heparin derivatives

2-O-desulfated and 6-O-desulfated heparins were prepared as reported previously [34, 35]. N-desulfated re-N-acetylated heparin was prepared by the method of Nagasawa et al. [36]. Totally desulfated heparin was prepared by the method of Sudo et al. [37]. Resulting heparin derivatives then were periodate-oxidized and borohydride-reduced as described for native heparin [32]. D-erythro-sphingosine was then attached to carboxylic groups of each product using the method described above to synthesize 2-ODSNP, 6-ODSNP, NDSNP, TDSNP respectively. In 2-ODSNP, 2-O-sulfoiduronic acid is converted to iduronic acid. This was observed by an upfield shift of H-1 signal from5.13 ppm to 4.90 and H-2 signal from 4.30 ppm to 4.17 ppm. In N-desulfonated samples the glucosamine H-2 signal of NAH assigned at 3.27 ppm completely disappeared, whereas a downfield shifted signal at 3.31 ppm appeared, which was the signal for H-2 bearing an -NH2 substituent. A chemical shift of 6-O-sulfoglucosamine H-1 (5.36 ppm) was observed upfield in 6-ODSNP compared to NAHNP (5.25 ppm). In totally desulfonated and re-N-acetylated nanoparticles (TDSNP), all the signals affected by N and O-sulfo groups on C-2 and C-3, C-6 of glucosamine and/or C-2 position of iduronic acid residues were found upfield compared to NAHNP.

2.3. Synthesis of NAH-Octadecanamine (NAHOCT), NAH-Decanamine (NAHDEC) and NAH-Pentanamine (NAHPEN) conjugates

NAH was first converted to chloroform soluble tetrabutylammonium salt. NAH (40 mg) was dissolved in water (80 mL) and passed through a Dowex 50WX8 (H + form, 200–400 mesh) column (0.8 × 10 cm) (Sigma-Aldrich) to exchange sodium ions to hydrogen ions. The acidic fraction was neutralized to pH 4.5with tetra-n-butylammonium hydroxide (40% in water) (Nacalai Tesque Inc., Kyoto, Japan) and lyophilized. NAH-tetrabutylammonium salt (20 mg) was then dissolved in chloroform (4 mL) following the addition of 5-fold molar excess of 1-ethyl-3-(3-dimethylaminopropyl)-carbodiimide and 1-octadecanamine (Sigma-Aldrich), 1-decanamine (Sigma-Aldrich) or 1-pentanamine (Sigma-Aldrich). The reaction mixture was stirred at room temperature for 24 h. Then, chloroform was evaporated in rotary evaporator followed by addition of 10% sodium hydrogen carbonate and the solution was kept at room temperature for 2 h. Then, the mixture was dialyzed against water and lyophilized as NAHOCT, NAHDEC or NAHPEN. Chemical shifts for attached 1-octadecanaminewere assigned at δ=0.87 (t, H18,-CH3), 1.20 (m, H-2-H-17, -CH2−), 2.90 (m, H-1, -CH2−), 8.04 (s, CO-NH). Chemical shifts for attached 1-decanamine were assigned at δ = 0.86 (t, H10, -CH3), 1.13 (t, H-3–H-9, -CH2−), 1.28 (m, H-2, -CH2−), 2.80 (t, H-1, -CH2−), 8.04 (s, CO-NH).

Chemical shifts for attached 1-pentanamine were assigned at δ=0.89 (t, H5, -CH3), 1.27 (m, H-2-H-4, -CH2−), 2.80 (m, H-1), 8.04 (s, CO-NH).

2.4. Particle size and zeta potential measurements

Size distribution and zeta potential values of nanoparticles were measured by Zetasizer Nano (Malvern Instruments, Worcestershire, UK).

2.5. Electron microscopy studies

Transmission electron microscopy (TEM) analysis was carried out using a HitachiH-7650microscope (Hitachi Co., Tokyo, Japan) operating at 80 kV accelerating voltage. Samples were prepared by placing a drop of nanoparticle solution (0.1 mg/mL) on a 400 mesh copper grid (Nisshin EM Co., Tokyo, Japan). Excess liquid was allowed to air-dry. Nanoparticles were then negatively stained with 2% w/v uranyl acetate solution. Images were captured using an AMT camera system.

2.6. Fluorescent probe studies

Critical micelle concentration (CMC) values of NAHNPs with different degrees of substitution by D-erythro-sphingosine were determined by fluorescence spectroscopy using pyrene as a probe, as described by Kabanov et al. [38]. Fluorescence spectra were recorded using a Fluoromax-4 spectrofluorometer (Horiba Ltd, Kyoto, Japan) at 25 °C. A solution of pyrene in acetone was added to vials and acetone was evaporated, depositing a thin film of pyrene to the vial wall. Conjugate solutions (3 mL) varying in concentration between 0.005 μg/mL and 1 mg/mL were then added to the flasks. The final pyrene concentration was 6.5 × 10−7 M. The solutions were equilibrated overnight at 35 °C. The excitation and emission wavelengths were 339 and 390nm, respectively. Spectra were accumulated with an integration time of 1 s/nm. Pyrene fluorescence intensity was plotted versus log concentrations of conjugates at 25 °C. The CMC values were taken from the intersection of the tangent to the curve at the inflection with the horizontal tangent through the points at low concentrations. The aggregation number of associating polymeric assemblies in nanoparticles was determined using a fluorescence quenching technique as reported previously [39]. Cetylpyridinium chloride (CPC) was used as a quencher for pyrene and prepared just before the experiments were performed. We also investigated hydrophobicity of the core of nanoparticles by measuring the partitioning coefficient of pyrene between the aqueous and micellar phases as described previously [38].

2.7. Cell isolation and in vitro assay for cytokines

Mouse peritoneal macrophages were isolated as described previously [40]. Briefly, cells were harvested from 5-week-old female ICR or C3H/HeJ mice 4 days after intraperitoneal injection

of 1 mL 2.9% thioglycollate medium (Nissui Pharmaceutical, Tokyo, Japan). Washed cells were suspended in RPMI 1640 medium supplemented with 10% fetal bovine serum (FBS) (Flow Laboratories, Irvine, UK), penicillin G (100 U/mL), and streptomycin (100 μg/mL), and then plated on 24-well plates (Falcon, Becton Dickinson, Lincoln Park, NJ, USA) at a density of 1.5 × 105 cells per well. After incubation for 2 h at 37 °C in a humidified atmosphere of 5% CO2 in air, non-adherent cells were washed off. The remaining cells were cultured for 24, 48, 72, or 96 h. After replacing the media with Opti-MEM® I Reduced Serum Medium (Gibco®, Life Technologies) containing nanoparticles (0.5 mg/mL final concentration) plus 20 ng/mL LPS (Sigma-Aldrich), cells were incubated for 24 h and the supernatant was assayed for cytokines using mouse TNF alpha ELISA kit (eBioscience, Inc.). Cells were also stimulated (where indicated) with 20 ng/mL PAM3CSK4 (InvivoGen), 20 ng/mL flagellin (InvivoGen) and 10 μg/mL poly(I:C) (InvivoGen) in the presence or absence of nanoparticles. IC50 value was calculated from the curve fitted to the dose–response inhibitory profile.

2.8. Western blotting

Peritoneal macrophages were cultured in a 100 mm culture dish in 10% FBS/RPMI 1640, and then medium was changed to Opti-MEM I. Next, cells were stimulated with LPS (20 ng/mL) in the presence or absence of NAHNP (0.5 mg/mL) for the indicated times. Cytosol and nuclear extracts were prepared using The Nuclear Extract Kit (Active Motif) and subjected to SDS-PAGE, transferred onto PVDV membrane (GE Healthcare) and probed with rabbit IgG antibodies against phospho-IRAK-1 (pThr209, Sigma-Aldrich), IκB-α (Santa Cruz Biotechnology, Inc.), p50 (Abcam plc) and RelA (Abcamplc). Blots were visualized using ImageQuant LAS 4000 (GE Healthcare).

2.9. Fluorescence-activated cell sorting (FACS) analysis

To analyze the interaction of NAHNP with TLR4/MD2, we performed FACS analysis using FITC (Sigma-Aldrich) labeled NAHNP (NAHNPFITC). Nanoparticles were labeled with FITC following the manufacturer's instructions and purified using ethanol precipitation method. Thioglycollate-elicited mouse peritoneal macrophages were maintained in 12-well plate (Falcon, Becton Dickinson, Lincoln Park, NJ, USA) at a density of 5.0 × 106 cells per well in 10% FBS/RPMI 1640 at 37 °C, 5% CO2 in a humidified atmosphere. Cells were then washed with PBS and incubated with anti-mouse TLR4/MD2 monoclonal antibody (MTS510, eBioscience, Inc.) in blocking buffer (PBS + 5%FBS) for 1 h to neutralize the receptor. After three washes with PBS cells were treated with NAHNP-FITC (0.1 mg/mL) in Opti- MEM® I Reduced Serum Medium and incubated for additional 30 min. Next, cells were washed with PBS three times and harvested by scraping for FACS analysis using BD FACS Canto II (BD Bioscience, Franklin Lakes, NJ, USA). As a positive control, cells were incubated with

NAHNP-FITC (0.1 mg/mL) in Opti-MEM® I for 30 min at room temperature without receptor neutralization step. After the specified time the cells were washed with PBS three times and processed to FACS analysis. Unstimulated cells served as a negative control.

2.10. Fluorescent microscopy

To further confirm the specificity of nanoparticles binding to TLR4/MD2, an immunofluorescence imaging experiment was conducted using fluorescent microscopy, in which macrophages were first treated with the allophycocyanin (APC) conjugated monoclonal anti-mouse TLR4/MD2 (APC-anti-TLR4/MD2) antibody. Macrophages were incubated with APC-anti-TLR4/MD2 in blocking buffer in 35 mm glass bottom dishes (Iwaki, Asahi Glass Co., Ltd, Japan) at a density of 2.0 × 104 cells/cm2 for 1 h. After three washes with PBS cells were treated with NAHNP-FITC (0.1 mg/mL) in Opti-MEM® I and incubated for additional 30 min and mounted in the same dish for microscopic visualization. Nuclei were stained by incubating cells with Hoechst 33342 (1 μg/mL) for 5 min prior to observation at room temperature. Positive control cells were treated with NAHNP-FITC (0.1 mg/mL) in Opti-MEM® I without TLR4/MD2 neutralization step and were incubated for 30 min before monitoring. We used Nikon Eclipse Ti inverted microscope equipped with A1R MP multiphoton confocal system (Nikon Instruments Inc., Tokyo, Japan) with hybrid scanning head which incorporates both a galvano scanner and an ultrahigh-speed resonant scanner. Images were processed with NIS Elements AR acquisition and analysis software (Nikon Instruments Inc., Tokyo, Japan).

2.11. In vitro cytotoxicity assay

Cell viability after nanoparticle treatment was determined using 2-(4-Iodophenyl)-3-(4-nitrophenyl)-5-(2,4-disulfophenyl)-2Htetrazolium salt (WST-1) based colorimetric assay according to the manufacturer's instructions (Roche Applied Biosystems).

2.12. Statistics

We used GraphPad Prism 5.0 (GraphPad Software, Inc.) to perform statistical tests. Data are presented as means ± SEM for each group. Experiments involving two groups were analyzed by two-tailed, unpaired t test. $P < 0.05$ was considered statistically significant.

3. Results

3.1. Synthesis and characterization of nanoparticles

NAH derivative was produced by glycol-splitting of C2\C3 bonds of nonsulfated D-glucuronic acid residues of native heparin [32, 41]. This also led to enhanced chain flexibility of the glycosaminoglycan (GAG) backbone. D-erythro-sphingosine was covalently attached to carboxylic groups of NAH (Fig. 1A). These conjugates self-assemble to form core-shell

nanoparticles above the CMC. TEM analysis demonstrated nanoparticles were uniformly spherical (Fig. 1B). Physicochemical characteristics of the nanoparticles are summarized in Table 1. Increasing the degree of substitution with D-erythro-sphingosine affected the physicochemical parameters of the nanoparticles by decreasing size and CMC (see Fig. 1C and Supplementary Fig. S1). Partitioning coefficient (K_p) of pyrene between the micellar and aqueous phases, an indicator of hydrophobicity, increased with increasing the degree of substitution (Supplementary Fig. S2). The aggregation number (n_{agg}) from fluorescent quenching measurements increased upon increasing the degree of substitution (Supplementary Fig. S3) whereas concurrently particles tended to decrease in size. Thus, lipid substitution strengthened hydrophobic interactions within the core. Zeta potential was highly negative indicating heparin chains covered the particles (Fig. 1D).

3.2. Effect of NAHNP on TLR4-mediated NF-κB signaling and production of TNF-α

The nanoparticles significantly inhibited in vitro production of TNF-α from E. coli lipopolysaccharide (LPS)-activated mouse peritoneal macrophages (Fig. 2A). Native heparin or NAH had no significant effect (Fig. 2B). Analysis of dose–response curves for NAHNP yielded the 50% inhibitory concentration (IC50) value of 0.019 mg/mL for inhibition of macrophage derived TNF-α production (Fig. 3). IC50 values were expressed as a percentage of the positive control and calculated as described above for the ELISA inhibition experiments. Inhibitory potency of nanoparticles with different degrees of substitution was not significantly different. To determine whether inhibition occurred by suppressing TLR4-mediated NF-κB signaling, the ability of NAHNP to inhibit cytokine release induced by specific extracellular TLR ligands was assessed. TNF-α production in response to TLR1/2 (Pam3CSK4), TLR3 (poly (I:C)) and TLR5 (flagellin) ligands was unaltered by NAHNP (Fig. 4A). NAHNP did not inhibit cytokine synthesis in macrophages with TLR4 mutations (TLR4Lps-d) isolated fromC3H/HeJ mice (Fig. 4B). TLR4Lps-d cells were unresponsive to LPS but did respond to Pam3CSK4, poly (I:C) or flagellin (Fig. 4B). The effect of NAHNP on activation of intracellular signaling molecules in the TLR4-mediated MyD88-dependent NF-κB pathway was examined. NAHNP prevented phosphorylation of interleukin-1 receptor-associated kinase-1 (IRAK-1), a signaling molecule downstream of MyD88 (Fig. 5). LPS-induced cytoplasmic degradation of inhibitor of NF-κB (IκBα) was blocked by NAHNP treatment. Nuclear extracts from LPS-treated cells revealed markedly suppressed nuclear localization of NF-κB p50/RelA subunits in the presence of NAHNP compared to controls (Fig. 5).

3.3. In vitro cytotoxicity of heparin nanoparticles

Nanoparticles were tested for cytotoxicity using primary cultured mouse peritoneal macrophages. Following 24 h of continuous exposure to the nanoparticles, cell viability was

determined usingWST-1 assay. Nanoparticles did not appear to be toxic (cell viability of greater than 80%) at concentrations up to 5mg/mL under tested conditions (Fig. 6).

3.4. Interaction of nanoparticles with TLR4/MD2

In order to confirm the interaction of NAHNP with the cell surface and to evaluate its TLR4/MD2 targeting specificity, the ligand–receptor binding of the nanoparticles was investigated using FACS and fluorescent microscopy. Binding of NAHNP-FITC to the cells was monitored with higher fluorescence signal; on the other hand, it was inhibited when TLR4/MD2 receptor complex was neutralized with anti-TLR4/MD2monoclonal antibody. The histograms of both conditions are compared in Fig. 7A. Interaction of the nanoparticles with TLR4/MD2 was further observed using fluorescent microscopy. As shown in Fig. 7B fluorescent signal of NAHNP-FITC was distributed over the cell surface (green in b, c) which was completely blocked by preincubation with APC-anti- TLR4/MD2 antibody (red in e, f). These results were consistent with the results of FACS analysis. We also evaluated the inhibitory effect of nanoparticles after 30min LPS-exposure and observed that nanoparticles inhibited TNF-α production from the macrophages at this time point (Fig. 7C). These results demonstrate that macrophages do not take up nanoparticles within 30 min, with the majority of nanoparticles being distributed over the surface of the cells and possessing the biological activity through TLR4/MD2 interaction.

3.5. Structure–activity relationship (SAR)

HPNP had a smaller anti-inflammatory effect than NAHNP in vitro (Fig. 8A) indicating the critical role of glycol-splitting. Glycol-splitting resulted in loss of anti-coagulant properties (data not shown) and significantly increased anti-inflammatory activity of nanoparticles. To explore the detailed SAR of nanoparticles, we examined the involvement of sulfo groups and the effect of alkyl chain length in the anti-inflammatory effect. A series of nanoparticles with regioselectively modified NAH were prepared. NAH was selectively 2-O-desulfated (2-ODSNP), 6-O-desulfated (6-ODSNP), N-desulfated re-N-acetylated (NDSNP) and totally desulfated (TDSNP) prior to D-erythro-sphingosine attachment to carboxylic groups of each derivative (Supplementary Fig. S4). In addition, conjugates where D-erythro-sphingosine of NAHNP was replaced with 1-octadecanamine (NAHOCT), 1- decanamine (NAHDEC) or 1-pentanamine (NAHPEN) was synthesized (Supplementary Fig. S5). To compare activities, TNF-α produced by mouse peritoneal macrophages treated with LPS in the presence or absence of test compounds was measured. Selective desulfation of N-sulfo (at C-2 of the D-glucosamine residues) and 2-O-sulfo (at C-2 of L-iduronic or D-glucuronic acid residues) groups did not affect the anti-inflammatory properties of NAHNP (Fig. 8B). In contrast, removal of 6- O-sulfate groups (at C-6 of D-glucosamine residues) reduced the anti-inflammatory potency. Thus, 6-O-sulfo groups contributed to the anti-inflammatory effect

(Fig. 8B). Totally desulfated nanoparticles retained an anti-inflammatory effect but were less effective than those with sulfo groups at C-6 position (Fig. 8B). Changes in the length of acyl chains altered the activity of NAHNP. Thus, NAHDEC and NAHPEN conjugates showed no inhibitory effect (Fig. 8C). All samples were pyrogen-free to avoid endotoxin contamination in vitro. Nanoparticles retained an inhibitory effect when D-erythro-sphingosine was replaced with lipids containing the same length of alkyl chain, such as 1- octadecanamine (Fig. 8C).

4. Discussion

We synthesized nanoparticles self-assembled from the amphiphilic conjugates of glycol-split heparin/D-erythro-sphingosine, which exhibit anti-inflammatory properties. Glycol-splitting of native heparin prior to conjugation with lipid strongly enhanced its anti-inflammatory properties. Nanoparticles possess high stability in aqueous solutions aggregating at low CMC of conjugates and have high hydrophobicity of inner core. However, their physicochemical characteristics are affected by the degree of substitution with D-erythro-sphingosine. Nanoparticles comprising a higher substituted conjugate (NAHNP10) could form more stable self-assemblies, thus might be more promising candidates for *in vivo* drug delivery and therapeutics. Anti-inflammatory effects of heparin were mediated through the ability of heparin to bind and inactivate proteins such as complement components, chemokines, growth factors, tissue destructive enzymes and adhesion molecules such as L- and P-selectins involved in recruitment of inflammatory cells [13, 14, 24]. In vitro studies showed that glycol-split heparin nanoparticles suppressed the production of TNF-α from LPS-stimulated macrophages by inhibiting TLR4-mediated NF-κB signaling with IC50 = 0.019 mg/mL. It is well known that interaction of LPS with TLR4–MD-2 receptor complexes results in activation of the MyD88-dependent downstream signaling pathway. This pathway induces the phosphorylation and degradation of IκBα, which in turn allows active NF-κB to translocate to the nucleus and induce proinflammatory cytokine gene expression. The recruitment and phosphorylation of IRAK1 is specific to the MyD88-dependent signaling pathway [42]. Early prevention of IRAK-1 phosphorylation by LPS treatment in the presence of NAHNP suggested the MyD88 signaling pathway was not activated. Interaction of NAHNP with TLR4/MD2 receptor complex was further confirmed by FACS analysis and visualized by fluorescent microscopy. We showed that inhibitory activity of nanoparticles was specific to cell surface TLR4/MD2, since no binding was detected after neutralization of the receptor. Furthermore, nanoparticles were effective against LPS stimulation of macrophages from the early minutes of exposure, when particles were observed to be accumulated over the cell surface. This is, to our knowledge, the first demonstration that lipid-modified heparin derivatives exhibit elevated anti-inflammatory properties by functioning as TLR4 antagonists through the TLR4–MyD88 pathway. Since the particles are covered with heparin chains, their surface charge is provided by sulfo and D-erythro-sphingosine unsubstituted carboxyl groups

and consequently, the most common type of interaction between surface heparins and their targets would be ionic. However, chain flexibility [43], non-electrostatic interactions such as hydrogen bonding and hydrophobic interactions also contribute to GAG–protein complex stability [44, 45]. Structure activity relationship studies were conducted to assess which chemical group in the nanoparticle heparin backbone might contribute to its anti-inflammatory activity. Blockade of L- and P-selectins require D-glucosamine 6-O-sulfation of the GAG chain in native heparin [24]. Our results showed that selective removal of 6-O-sulfo groups at C-6 of D-glucosamine decreased its activity. The TLR4–MD-2 receptor complex has affinity with amphiphilic lipid A and its analogs, and is sensitive to the nature and length of acyl chains and the interaction with charged groups on the hydrophilic portion of ligands [46–48]. Crystal structures of antagonistic (lipid IVa, Eritoran) binding to TLR4–MD-2 show that di-glucosamine residues do not interact directly with MD-2 whereas lipid chains interact with MD-2 through hydrophobic contacts. D-erythro-sphingosine chains of NAHNP could interact in a similar manner to those of acyl chains in TLR4 synthetic antagonists whereas decreased chain lengths of NAHNP may affect these interactions, resulting in loss of inhibitory activity. However, detailed structural analysis is required to reveal the role of ionic interactions of 6-O-sulfo groups and evaluate receptor ligand interactions at the molecular level.

5. Conclusion

We show that glycol-split heparin conjugated with alkyl amines forms stable self-assembling nanoparticles in aqueous solutions. These nanoparticles exhibit anti-inflammatory effect and effectively suppress TNF-α from LPS-stimulated macrophages. This effect is mediated through the inhibition of the TLR4–NF-κB pathway. This is to our knowledge, the first report showing that lipid-modified heparin derivatives possess elevated anti-inflammatory properties by functioning as TLR4 antagonists. SAR analysis of these non-anticoagulant heparin nanoparticles revealed the importance of 6-O-sulfo group and the length of alkyl chain of attached hydrophobic moiety in anti-inflammatory activity. However, additional pharmacological and toxicological studies are required to evaluate whether the nanoparticles can be used in clinical settings.

Acknowledgments

This research was supported in part by a Grant-in-Aid for Challenging Exploratory Research (23659022, F.Y.) from the Ministry of Education, Culture, Sports, Science & Technology, Japan.

Table 1. Characterization of nanoparticles

	Molar ratio[a]	Size (nm)	ζ-potential (mV)	PDI[b]	DS[c]	n_{agg}[d]	CMC[e] (μg/mL)	K_p[f]	ν[g], (cm^3/g)
NAHNP1	1:1	160±2.6	–55.6±2.1	0.29±0.03	3.57	30.5±2.8	0.47	$8.1 \cdot 10^4$	0.68
NAHNP10	1:10	110±3.4	–30.1±1.7	0.32±0.02	8.20	77.4±4.9	0.013	$1.0 \cdot 10^5$	0.70

[a]Molar ratio of NAH:D-erythro-sphingosine. [b]Polydispersity index. [c]Degree of substitution of D-erythro-sphingosine. [d]Aggregation number per one hydrophobic domain. [e]Criticalmicellar concentration. [f]Partitioning coefficient of pyrene in distilled water in presence of NAHNP conjugates. [g]Partial specific volume in water at 25 °C determined using a pycnometer. Results are means ±SD from triplicate experiments.

Figure legends

Fig. 1. Structure and formation of non-anticoagulant heparin nanoparticles. (A) Chemical structure of NAHNP. (B) Nanoparticles were stained with uranyl acetate and visualized using transmission electron microscopy. Scale bar: 100 nm. (C) Particle size distribution of NAHNP1 (top) and NAHNP10 (bottom) in water after 1 min ultrasonication. (D) Zeta potential distribution of NAHNP1 (top) and NAHNP10 (bottom).

Fig. 2. Inhibitory effect of NAHNP on *in vitro* production of TNF-α via TLR4. Quantification of TNF-α from peritoneal macrophages isolated from wild-type mice. Cells (1.5×10^5 cells per well) were seeded to 24-well-plates and were not treated (NT) or stimulated with LPS (20 ng/mL) for 24 hours in the presence or absence of 0.5 mg/mL NAHNP (A), native heparin or NAH (B). Data are shown as mean ±SEM (n=3). ** $P \leq 0.01$.

Fig. 3. Dose-dependent effect of NAHNP on TNF-α production from LPS-stimulated macrophages after 24h. The results are given as mean ±SEM (n=3), by expressing the inhibition of cytokine-producing cells as a percentage of LPS-stimulated non-drug-exposed macrophages. Non-stimulated cells were used as negative controls.

Fig. 4. NAHNP fails to inhibit TNF-α production in TLR1/2, TLR3 or TLR5 activated macrophages. Quantification of TNF-α from peritoneal macrophages isolated from wild-type mice (A) and mutant $TLR4^{Lps\text{-}d}$ mice (B). Cells (1.5×10^5 cells per well) were seeded to 24-well-plates and were not treated (NT) or stimulated with LPS (20 ng/mL), poly (I:C) (10μg/mL), flagellin (20 ng/mL) or PAM3CSK4 (20 ng/mL) for 24 hours in the presence or absence of 0.5 mg/mL NAHNP. Data are shown as mean ±SEM (n=3).

Fig. 5. Effect of NAHNP on activation of downstream proteins of TLR4–NF-κB signaling pathway. Primary macrophages were stimulated with LPS (20 ng/mL) in the presence (+) or absence (–) of NAHNP (0.5 mg/mL) for the indicated times. Cytosolic and nuclear extracts analyzed by western blot using antibodies directed against p-IRAK1, IκBα, RelA and p50. β-actin served as loading control.

Fig. 6. Concentration-dependent cytotoxicity of NAHNP in thioglycollate-elicited peritoneal macrophages. Cells (1.0×10^5 cells per well) were seeded to 96-well-plates and were continuously exposed to nanoparticles at indicated concentrations for 24h in Opti-MEM® I. Cell viability was measured by the WST-1 assay. The data are plotted as the percentage of absorbance in comparison with untreated controls and shown as mean ±SEM (n=4).

Fig. 7. Evaluation of binding of nanoparticles to TLR4/MD2 receptor complex. (A) Representative overlay histogram of a FACS experiment: no fill, unlabeled macrophages; red fill, macrophages were stained with NAHNP-FITC for 30 min at 37°C; gray fill, macrophages were preincubated with anti-TLR4/MD2 antibody for 1 h at 37°C and stained with NAHNP-FITC for 30 min. Shown are results from 1 of 3 representative experiments. (B) Fluorescence microscope images of living macrophages. (a-c) Cells were incubated with NAHNP-FITC

(green in b, c) for 30 min at 37°C. (d-f) Cells were pretreated with APC conjugated anti-TLR4/MD2 antibody (red in e, f) for 1 h at 37°C before washing and incubating with NAHNP-FITC for 30 min. Hoechst 33342 staining (blue) was used to detect cell nuclei. Scale: 50μm. (C) Quantification of TNF-α from peritoneal macrophages. Cells (1.0×10^6 cells per well) were seeded to 24-well-plates and were not treated (NT) or stimulated with LPS (20 ng/mL) for 30 min in the presence or absence of 0.1 mg/mL NAHNP-FITC. Data are shown as mean ±SEM (n=3). ** $P \leq 0.01$.

Fig. 8. Structure activity relationship data. Effect of glycol-splitting (A), 2-ODSNP, NDSNP, 6-ODSNP, TDSNP (B), NAHDEC, NAHPEN and NAHOCT (C) on TNF-α production from LPS stimulated mouse peritoneal macrophages. Cells (1.5×10^5 cells/well) were seeded to 24-well plate and were not treated (NT) or stimulated with LPS (20 ng/mL) with or without chemically-modified heparin derivatives (0.5 mg/mL) for 24 hours. Data are shown as mean ±SEM (n=3). *** $P \leq 0.001$.

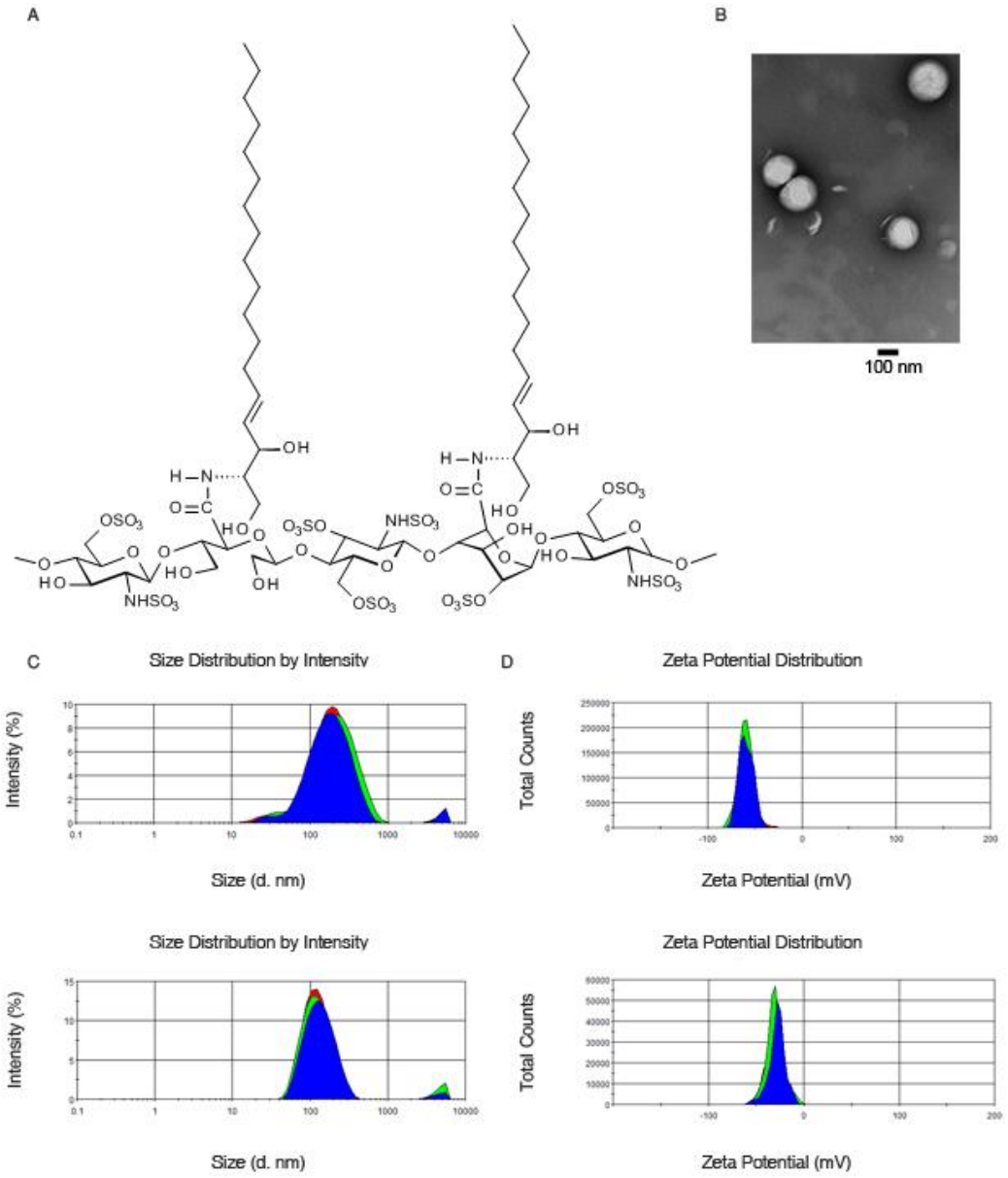

Fig. 1. Structure and formation of non-anticoagulant heparin nanoparticles.

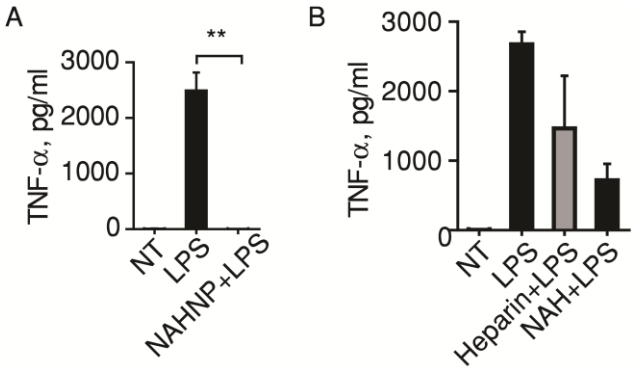

Fig. 2. Inhibitory effect of NAHNP on *in vitro* production of TNF-α via TLR4.

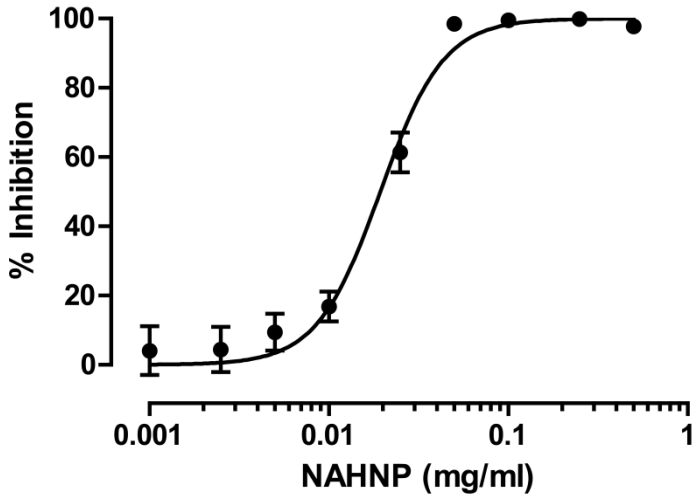

Fig. 3. Dose-dependent effect of NAHNP on TNF-α production from LPS-stimulated macrophages after 24h.

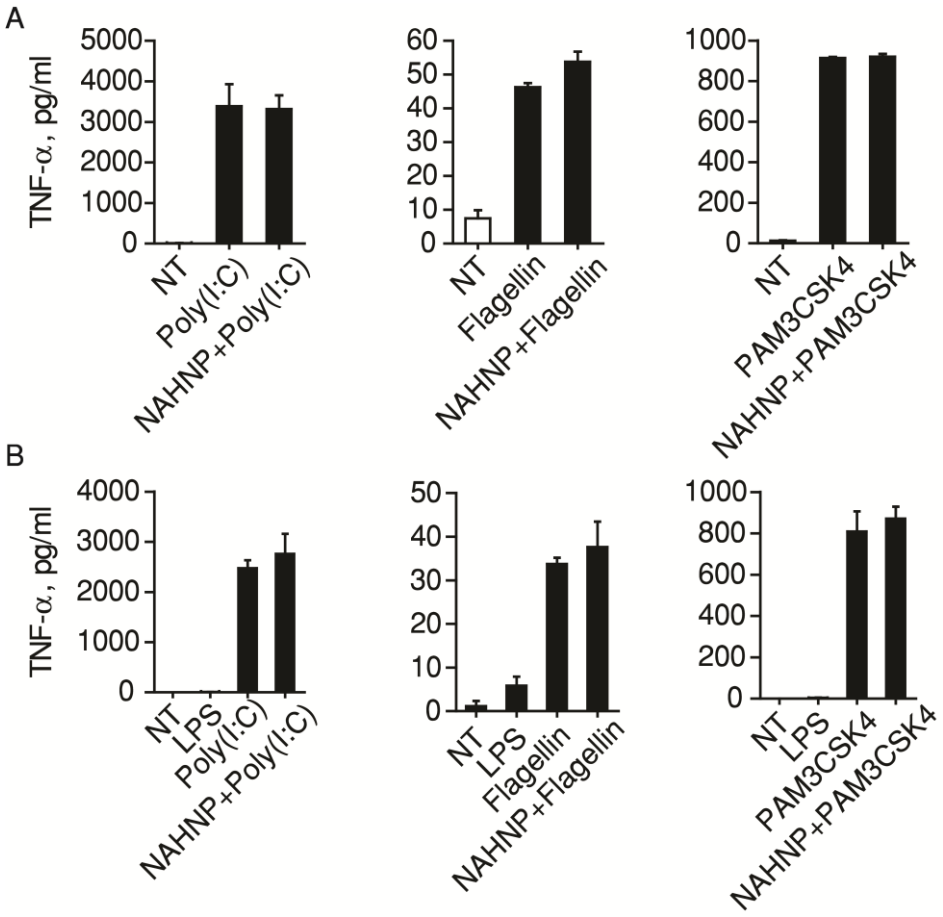

Fig. 4. NAHNP fails to inhibit TNF-α production in TLR1/2, TLR3 or TLR5 activated macrophages.

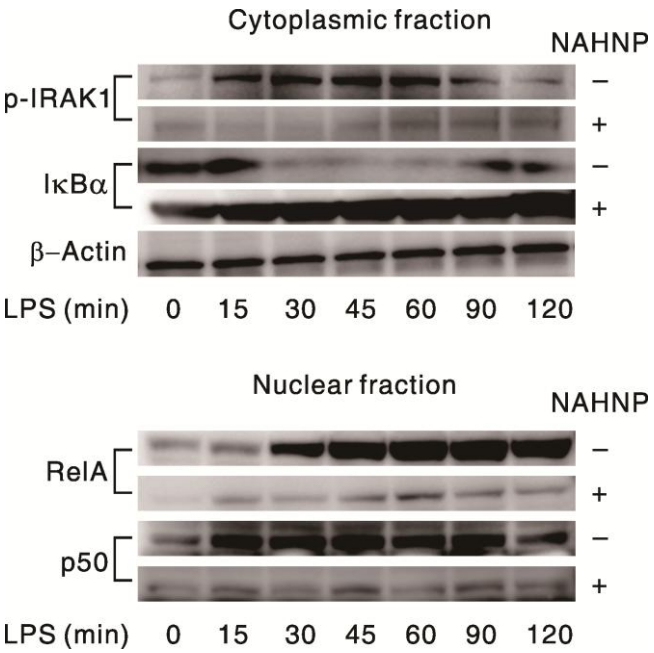

Fig. 5. Effect of NAHNP on activation of downstream proteins of TLR4–NF-κB signaling pathway.

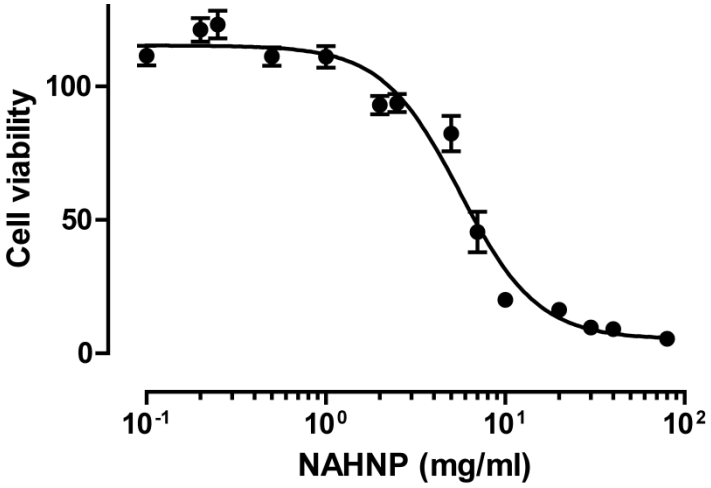

Fig. 6. Concentration-dependent cytotoxicity of NAHNP in thioglycollate-elicited peritoneal macrophages.

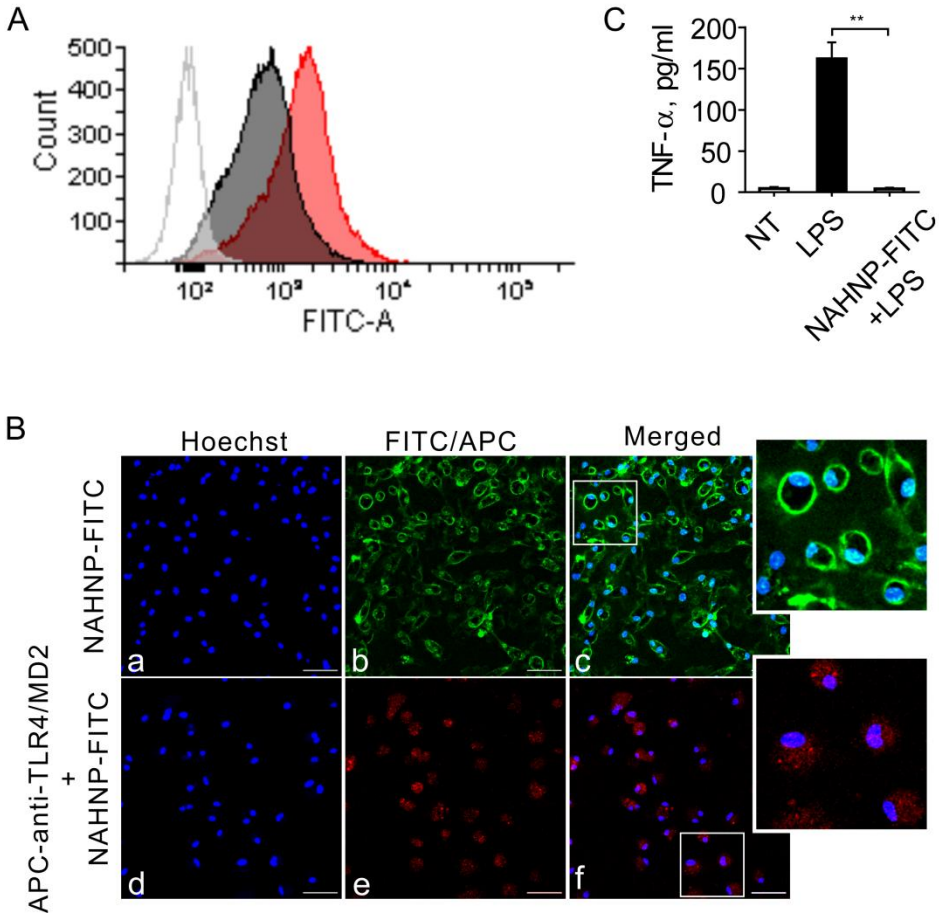

Fig. 7. Evaluation of binding of nanoparticles to TLR4/MD2 receptor complex.

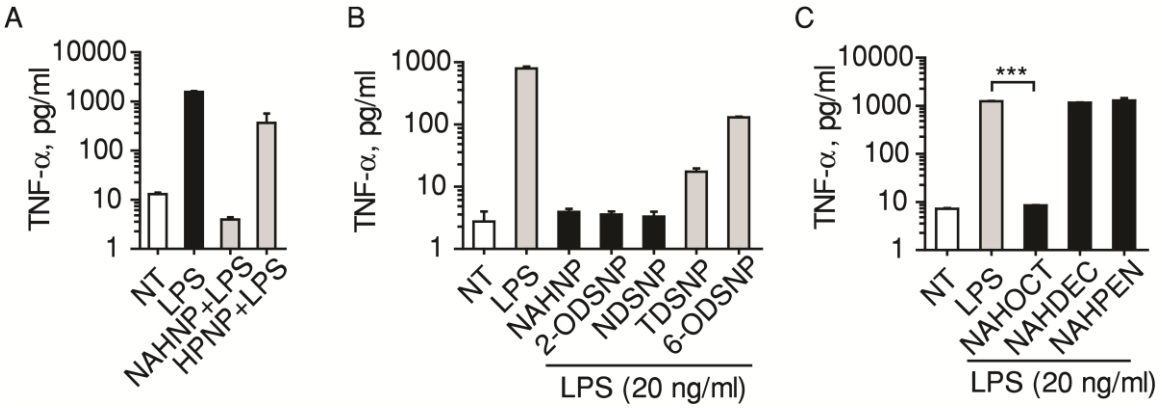

Fig. 8. Structure activity relationship data.

References

[1] M.M. Kemp, R.J. Linhardt, Heparin-based nanoparticles, Wiley Interdiscip. Rev. Nanomed. Nanobiotechnol. 2 (2010) 77–87.

[2] C. Chauvierre, D. Labarre, P. Couvreur, C. Vauthier, Novel polysaccharide-decorated poly(isobutyl cyanoacrylate) nanoparticles, Pharm. Res. 20 (2003) 1786–1793.

[3] C. Passirani, G. Barratt, J.-P. Devissaguet, D. Labarre, Interactions of nanoparticles bearing heparin or dextran covalently bound to poly(methyl methacrylate) with the complement system, Life Sci. 62 (1998) 775–785.

[4] C. Passirani, G. Barratt, J.-P. Devissaguet, D. Labarre, Long-circulating nanoparticles bearing heparin or dextran covalently bound to poly(methyl methacrylate), Pharm. Res. 15 (1998) 1046–1050.

[5] K. Park, G.Y. Lee, Y.S. Kim, M. Yu, R.W. Park, I.S. Kim, S.Y. Kim, Y. Byun, Heparindeoxycholic acid chemical conjugate as an anticancer drug carrier and its antitumor activity, J. Control. Release 114 (2006) 300–306.

[6] C. Chauvierre, M.C. Marden, C. Vauthier, D. Labarre, P. Couvreur, L. Leclerc, Heparin coated poly(alkylcyanoacrylate) nanoparticles coupled to hemoglobin: a new oxygen carrier, Biomaterials 25 (2004) 3081–3086.

[7] C. Chauvierre, C. Vauthier, D. Labarre, M.C. Couvreur, L. Leclerc, A new generation of polymer nanoparticles for drug delivery, Cell. Mol. Biol. 50 (2004) 233–239.

[8] M.M. Kemp, A. Kumar, S. Mousa, T.-J. Park, P. Ajayan, N. Kubotera, S.A. Mousa, R.J. Linhardt, Synthesis of gold and silver nanoparticles stabilized with glycosaminoglycans having distinctive biological activities, Biomacromolecules 10 (2009) 589–595.

[9] Z. Liu, Y. Jiao, F. Liu, Z. Zhang, Heparin/chitosan nanoparticle carriers prepared by polyelectrolyte complexation, J. Biomed. Mater. Res. 83A (2007) 806–812.

[10] Y.-H. Lin, C.-H. Chang, Y.-S.Wu, Y.-M. Hsu, S.-F. Chiou, Y.J. Chen, Development of pH responsive chitosan/heparin nanoparticles for stomach-specific anti-Helicobacter pylori therapy, Biomaterials 30 (2009) 3332–3342.

[11] S.H. Choi, J.-H. Lee, S.-M. Choi, T.G. Park, Thermally reversible pluronic/heparin nanocapsules exhibiting 1000-fold volume transition, Langmuir 22 (2006) 1758–1762.

[12] H. Khurshid, S.H. Kim, M.J. Bonder, L. Colak, B. Ali, S.I. Shah, K.L. Kiick, G.C. Hadjipanayis, Development of heparin-coated magnetic nanoparticles for targeted drug delivery applications, J. Appl. Phys. 105 (2009) (07B308/1–07B308/3).

[13] D.J. Tyrrell, A.P. Horne, K.R. Holme, J.M. Preuss, C.P. Page, Heparin in inflammation: potential therapeutic applications beyond anticoagulation, Adv. Pharmacol. 46 (1999) 151–208.

[14] R.J. Ludwig, Therapeutic use of heparin beyond anticoagulation, Curr. Drug Discov. Technol. 6 (2009) 281–289.

[15] R. Lever, C.P. Page, Novel drug development opportunities for heparin, Nat. Rev. Drug Discov. 1 (2002) 140–148.

[16] S.M. Lord, B. Tsoi, C. Gunawan, W.Y. Teoh, R. Amal, J.M. Whitelock, Anti-angiogenic activity of heparin functionalised cerium oxide nanoparticles, Biomaterials 34 (2013) 8808–8818.

[17] K. Park, Y.S. Kim, G.Y. Lee, J.O. Nam, S.K. Lee, R.W. Park, S.Y. Kim, I.S. Kim, Y. Byun, Antiangiogenic effect of bile acid acylated heparin derivative, Pharm. Res. 24 (1) (2007) 176–185.

[18] D.Y. Lee, S.K. Kim, Y.S. Kim, D.H. Son, J.H. Nam, I.S. Kim, R.W. Park, S.Y. Kim, Y. Byun, Suppression of angiogenesis and tumor growth by orally active deoxycholic acid heparin conjugate, J. Control. Release 118 (2007) 310–317.

[19] J.W. Park, O.C. Jeon, S.K. Kim, T.A. Al-Hilal, S.J. Jin, H.T. Moon, V.C. Yang, S.Y. Kim, Y. Byun, High antiangiogenic and lowanticoagulant efficacy of orally active lowmolecular weight heparin derivatives, J. Control. Release 148 (2010) 317–326.

[20] A. Gaffney, P. Gaffney, Rheumatoid arthritis and heparin, Br. J. Rheumatol 35 (1996) 808.

[21] P.R. Gaffney, C.T. Doyle, A. Gaffney, J. Hogan, D.P. Hayes, P. Annis, Paradoxical response to heparin in 10 patients with ulcerative colitis, Am. J. Gastroenterol. 90 (1995) 220–223.

[22] C. Vancheri, C. Mastruzzo, F. Armato, V. Tomaselli, S. Magrì, M.P. Pistorio, M. LaMicela, L. D amico, N. Crimi, Intranasal heparin reduces eosinophil recruitment after nasal allergen challenge in patients with allergic rhinitis, J. Allergy Clin. Immunol. 108 (2001) 703–708.

[23] E. Young, The anti-inflammatory effects of heparin and related compounds, Thromb. Res. 122 (6) (2008) 743–752.

[24] L. Wang, J.R. Brown, A. Varki, J.D. Esko, Heparin's anti-inflammatory effects require glucosamine 6-O-sulfation and are mediated by blockade of L- and P-selectins, J. Clin. Invest. 110 (2002) 127–136.

[25] S. Akira, K. Takeda, T. Kaisho, Toll-like receptors: critical proteins linking innate and acquired immunity, Nat. Immunol. 2 (2001) 675–680.

[26] A.N. Theofilopoulos, R. Gonzalez-Quintial, B.R. Lawson, Y.T. Koh, M.E. Stern, D.H. Kono, B. Beutler, R. Baccala, Sensors of the innate immune system: their link to rheumatic diseases, Nat. Rev. Rheumatol. 6 (2010) 146–156.

[27] S.Walter,M. Letiembre, Y. Liu, H. Heine, B. Penke, W. Hao, B. Bode, N.Manietta, J.Walter, W. Schulz-Schuffer, K. Fassbender, Role of the toll-like receptor 4 in neuroinflammation in Alzheimer's disease, Cell. Physiol. Biochem. 20 (2007) 947–956.

[28] T.L. Suber, L. Casciola-Rosen, A. Rosen,Mechanisms of disease: autoantigens as clues to the pathogenesis of myositis, Nat. Rev. Rheumatol. 4 (2008) 201–209.

[29] A. Lartigue, N. Colliou, S. Calbo, A. François, S. Jacquot, C. Arnoult, F. Tron, D. Gilbert, P. Musette, Critical role of TLR2 and TLR4 in autoantibody production and glomerulonephritis in lpr mutation-induced mouse lupus, J. Immunol. 183 (2009) 6207–6216.

[30] Jennifer L. Stow, Pei Ching Low, Carolin Offenhäuser, Daniele Sangermani, Cytokine secretion inmacrophages and other cells: pathways andmediators, Immunobiology 214 (2009) 601–612.

[31] J.M. Cavaillon, Cytokines and macrophages, Biomed. Pharmacother. 48 (1994) 445–453.

[32] H.E. Conrad, Y. Guo, Structural analysis of periodate-oxidized heparin, Adv. Exp. Med. Biol. 313 (1992) 31–36.

[33] P.K. Smith, A.K. Mallia, G.T. Hermanson, Colorimetric method for the assay of heparin content in immobilized heparin preparations, Anal. Biochem. 109 (1980) 466.

[34] H.G. Garg, H. Mrabat, L. Yu, C. Freeman, B. Li, F. Zhang, R.J. Linhardt, C.A. Hales, Significance of the 2-O-sulfo group of L-iduronic acid residues in heparin on the growth inhibition of bovine pulmonary artery smooth muscle cells, Carbohydr. Res. 343 (2008) 2406–2410.

[35] Y. Kariya,M. Kyogashima, K. Suzuki, T. Isomura, T. Sakamoto, K. Horie, M. Ishihara, R. Takano, K. Kamei, S. Hara, Preparation of completely 6-O-desulfated heparin and its ability to enhance activity of basic fibroblast growth factor, J. Biol. Chem. 275 (2000) 25949–25958.

[36] K. Nagasawa, Y. Inoue, T. Kamata, Solvolytic desulfation of glycosaminoglycuronan sulfates with dimethyl sulfoxide containing water or methanol, Carbohydr. Res. 58 (1977) 47–55.

[37] M. Sudo, K. Sato, A. Chaidedgumjorn, H. Toyoda, T. Toida, T. Imanari, 1H nuclear magnetic resonance spectroscopic analysis for determination of glucuronic and iduronic acids in dermatan sulfate, heparin, and heparan sulfate, Anal. Biochem. 297 (2001) 42–51.

[38] A.V. Kabanov, R.I. Nazarova, I.V. Astafieva, E.V. Batrakova, V.Yu. Alakhov, A.A. Yaroslavov, V.A. Kabanov,Micelle formation and solubilization of fluorescent probes in poly(oxyethylene-b-oxypropylene-b-oxyethylene) solutions,Macromolecules 28 (1995) 2303–2314.

[39] K. Akiyoshi, S. Deguchi, H. Tajima, T. Nishikawa, J. Sunamoto, Microscopic structure and thermoresponsiveness of a hydrogel nanoparticle by self-assembly of a hydrophobized polysaccharide, Macromolecules 30 (1997) 857–861.

[40] W. Yeeprae, S. Kawakami, F. Yamashita, M. Hashida, Effect of mannose density on mannose receptor-mediated cellular uptake of mannosylated O/W emulsions by macrophages, J. Control. Release 114 (2006) 193–201.

[41] B. Casu, G. Diamantini, G. Fedeli, M. Mantovani, P. Oreste, R. Pescador, R. Porta, G. Prino, G. Torri, G. Zoppetti, Retention of antilipemic activity by periodateoxidized non-anticoagulant heparins, Arzneimittelforschung 36 (1986) 637–642.

[42] Q. Li, I.M. Verma, NF-kappaB regulation in the immune system, Nat. Rev. Immunol. 2 (2002) 725–734.

[43] R.J. Linhardt, Claude S. Hudson, Award address in carbohydrate chemistry. Heparin: structure and activity, J. Med. Chem. 46 (2003) 2551–2564.

[44] J. Bae, U.R. Desai, A. Pervin, E.E. Caldwell, J.M. Weiler, R.J. Linhardt, Interaction of heparin with synthetic antithrombin III peptide analogues, Biochem. J. 301 (1994) 121–129.

[45] R.E. Hileman, R.N. Jennings, R.J. Linhardt, Thermodynamic analysis of the heparin interaction with a basic cyclic peptide using isothermal titration calorimetry, Biochemistry 37 (1998) 15231–15237.

[46] J.Y. Homma, M. Matsuura, Y. Kumazawa, Structure–activity relationship of chemically synthesized nonreducing parts of lipid A analogs, Adv. Exp. Med. Biol. 256 (1990) 101–119.

[47] Y. Fujimoto, Y. Adachi, M. Akamatsu, Y. Fukase, M. Kataoka, Y. Suda, K. Fukase, S. Kusumoto, Synthesis of lipid A and its analogues for investigation of the structural basis for their bioactivity, J. Endotoxin Res. 11 (2005) 341–347.

[48] B.S. Park, D.H. Song, H.M. Kim, B.S. Choi, H. Lee, J.O. Lee, The structural basis of lipopolysaccharide recognition by the TLR4-MD-2 complex, Nature 458 (2009) 1191–1195.

Self-assembling lipid modified non-anticoagulant heparin nanoparticles suppress lipopolysaccharide-induced inflammation through TLR4–NF-κB signaling

Hasan Babazada[1], Fumiyoshi Yamashita[1], Shinya Yanamoto[1] and Mitsuru Hashida[1, 2*]

[1]Department of Drug Delivery Research, Graduate School of Pharmaceutical Sciences, Kyoto University, Yoshidashimoadachi-cho, Sakyo-ku, Kyoto 606-8501, Japan.

[2]Institute for Integrated Cell-Material Sciences, Kyoto University, Yoshidaushinomiya-cho, Sakyo-ku, Kyoto 606-8501, Japan.

*Corresponding author info:
Tel: 81-75-753-4535
Fax: 81-75-753-4575
E-mail: hashidam@pharm.kyoto-u.ac.jp

Conflict of interest

Authors declare no conflict of interest.

Supplementary data

Determination of critical micelle concentration (CMC) of NAHNP

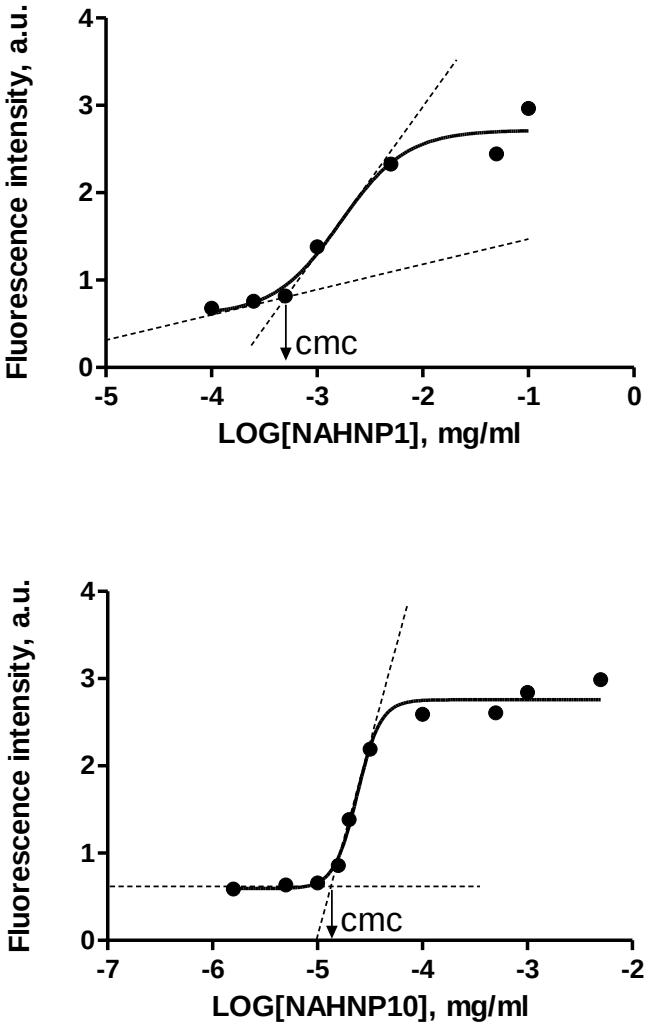

Supplementary Fig. S1. Plot of pyrene fluorescence intensity versus log concentrations of NAHNP1 with DS 3.57% (top) and NAHNP10 with DS 8.20% (bottom) at 25°C.

Determination of partitioning coefficient of pyrene in NAHNP solutions

Partitioning equilibrium between micellar and water phases can be determined using the formula:

$$P = \frac{[Py]_m}{[Py]_w}$$

where $[Py]_m$ and $[Py]_w$ are pyrene concentrations in the micellar and aqueous phases, respectively. The emission in NAHNP solutions is the sum of the emissions of probe in aqueous and micellar phases and can be expressed as follows:

$$(I_{max} - I)/(I - I_0) = \frac{1 + (P-1)\theta}{\theta P}$$

where θ is the volume portion of the micellar phase (θ=0.001ν ([NAHNP]-CMC)); and I_0 and I_{max} are the intensities of pyrene at lower and higher concentrations of NAHNP. The experimental plots corresponding to this relationship are presented in **Supplementary Fig. S2** and K_p values are determined from the slope of the experimental curves.

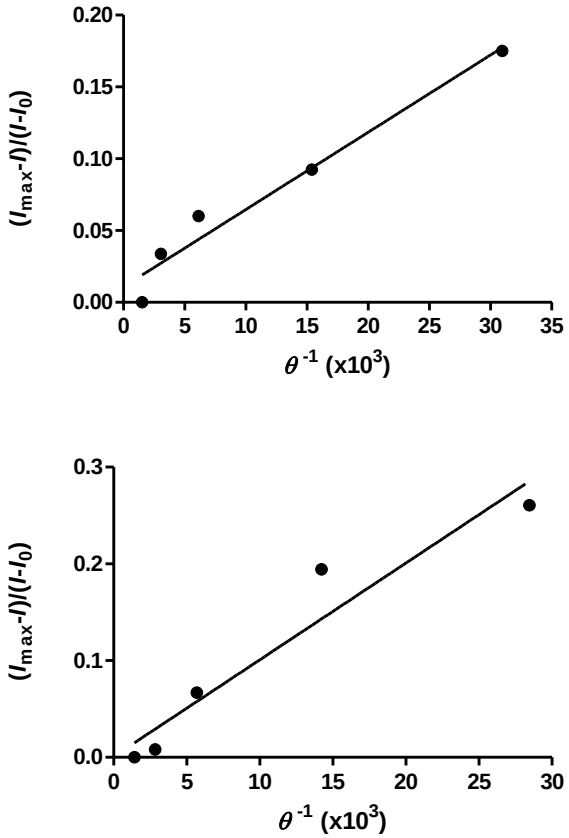

Supplementary Fig. S2. Plot of $(I_{max}-I)/(I-I_0)$ versus θ^1 obtained for pyrene (λ_{ex}=339 nm, λ_{em}=390 nm.) solubilized in NAHNP1 with DS 3.57% (top) and NAHNP10 with DS 8.20% (bottom).

Determination of aggregation number of NAHNP

The steady-state quenching data in microheterogeneous systems such as aqueous-micellar solution do not fit simple Stern-Volmer kinetics, but have the following quenching kinetics:

$$\ln(I_0/I)=[Q]/[M]$$

where I and I_0 are fluorescence intensities in the presence and absence of the quencher, [Q] is the bulk concentration of the quencher and [M] is the concentration of self-assemblies.

Plot of $\ln(I_0/I)$ versus the concentration of CPC gives a straight line (**Supplementary Fig. S3**). The slope corresponds to 1/[M]. Thus, n_{agg} can be calculated by:

n_{agg}= [D-erythro-sphingosine]/[M]

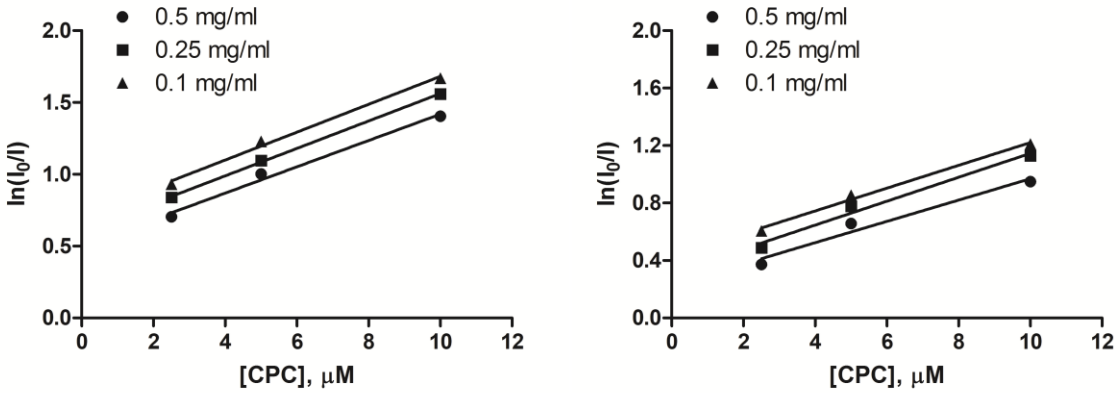

Supplementary Fig. S3. $\ln(I_0/I)$ of pyrene fluorescence as a function of CPC concentration in the presence of NAHNP1 with DS 3.57% (left) and NAHNP10 with DS 8.20% (right) at indicated concentrations.

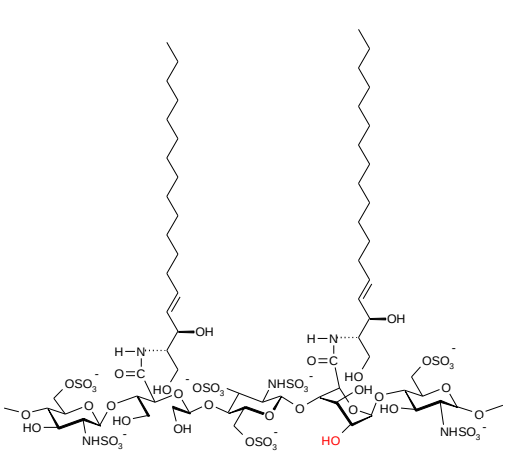

2-ODSNP

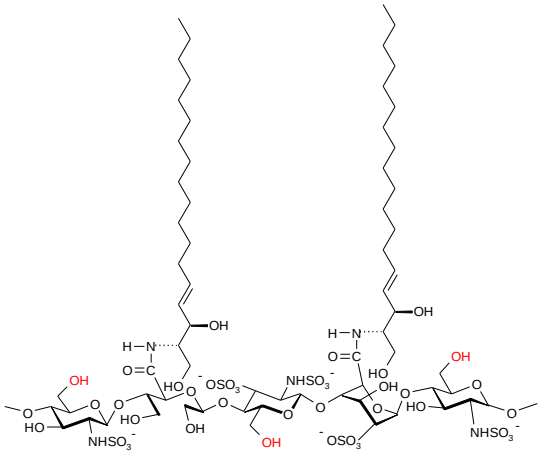

6-ODSNP

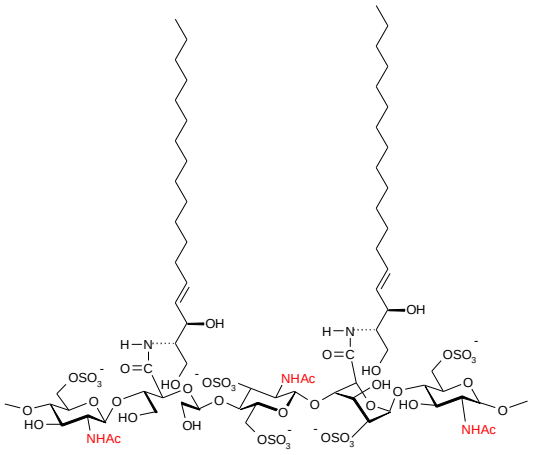

NDSNP

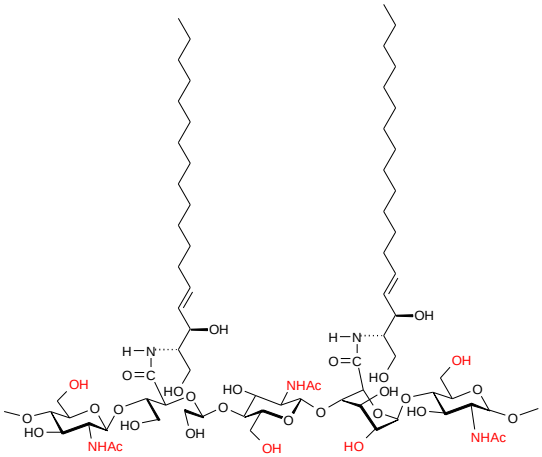

TDSNP

Supplementary Fig. S4. Chemical structures of compounds. D-erythro-sphingosine was attached to carboxylic groups of selectively 2-O-desulfated (2-ODSNP), 6-O-desulfated (6-ODSNP), N-desulfated re-N-acetylated (NDSNP) and totally desulfated (TDSNP) glycol-split heparin.

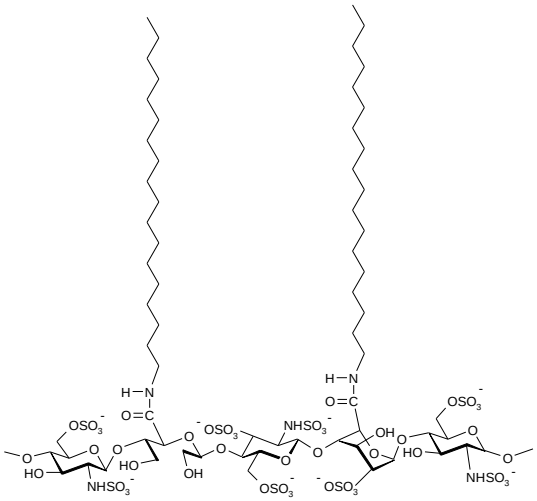

NAHOCT

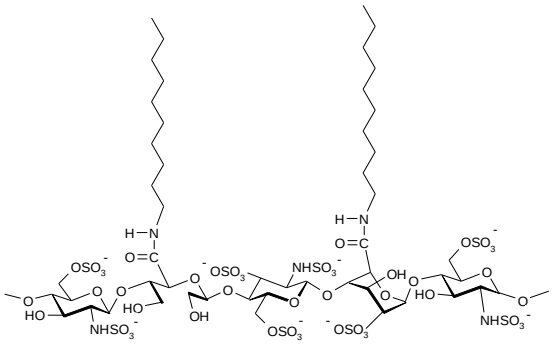

NAHDEC

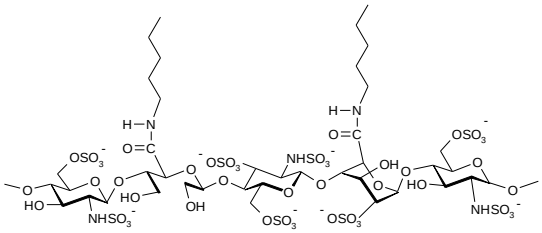

NAHPEN

Supplementary Fig. S5. Structures of lipid modified NAH derivatives. D-erythro-sphingosine of NAHNP was replaced with 1-octadecanamine (NAHOCT), 1-decanamine (NAHDEC) or 1-pentanamine (NAHPEN) .